物 理 化 学 学 报

Acta Phys. -Chim. Sin. **2024,** *40* (X), 2304027 (1 of 8)

[Article] doi: 10.3866/PKU.WHXB202304027 www.whxb.pku.edu.cn

Photothermal Microscopy of Graphene Flakes with Different Thicknesses

Anbang Du †, Yuanfan Wang †, Zhihong Wei †,*, Dongxu Zhang, Li Li, Weiqing Yang, Qianlu Sun, Lili Zhao, Weigao Xu *, Yuxi Tian *

Key Laboratory of Mesoscopic Chemistry of MOE, School of Chemistry and Chemical Engineering, Jiangsu Key Laboratory of Vehicle Emissions Control, Nanjing University, Nanjing 210023, China.

Abstract: Two-dimensional (2D) layered materials have attracted widespread research interest and have significantly promoted the development of chemistry, material science, and condensed matter physics. Since the emergence of graphene, 2D materials with unique mechanical, thermal, optical, and electrical properties have been developed. In the case of graphene, its extraordinary mechanical strength, carrier mobility, thermal conductivity, and light-absorption over the whole spectral range in UV-Vis and near infrared guarantee a wide range of prospective applications. The electronic structure and properties of graphene flakes are dominated by their thickness, twist angle, and dielectric environment. Tailoring the interlayer interactions of graphene layers can provide additional opportunities for developing optical and electrical nanodevices, resulting in pioneering outcomes, such as the magic-angle graphene. Over the past decade, one of the most active research directions in the field of 2D materials has been the development of novel techniques that can probe the thickness-dependent physical properties of layered materials. In contrast with the intensively studied mechanical, electrical, and optical properties, microscopic investigations of the thermal characteristics of graphene flakes remain to be explored. Photothermal (PT) microscopy is a new all-optical microscopic imaging technique that has gained substantial attention and undergone long-term development in recent years, especially in the fields of nanomaterials and life sciences. The fundamental principle of PT microscopy is to heat the target sample based on the absorption of a heating beam and use a probe beam to indirectly capture information on microscale heat generation and transport. Inspired by several pioneering studies, we conducted a comparative study of the thickness-dependent PT properties of mechanically exfoliated graphene flakes in two different PT media, *i.e.*, air and glycerol. Whereas a nonlinear relationship between the PT intensity and sample thickness was observed in both media, the PT intensities from the two media were distinct. A high-contrast and non-monotonic PT response was observed in glycerol. The PT intensity of monolayer graphene was higher than that of bilayer graphene, and the PT intensities of graphene flakes with 2–4 layers exhibited a good linear relationship with the thickness. We also analyzed the relationship between the PT intensity and heating or probe power, demonstrating that the PT intensity as well as the absorption cross-section of graphene derived from the PT signal vary linearly with the power of both laser beams. Our study provides insights into light absorption and thermal relaxation features of graphene flakes of different thicknesses, which can guide future studies on the thermal properties of layered materials and their heterostructures.

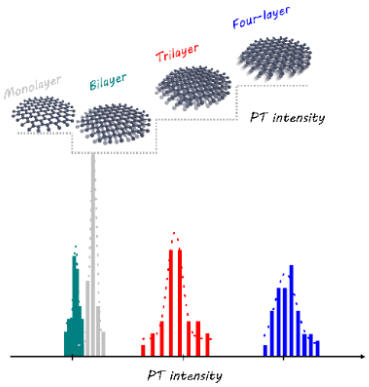

Received: April 14, 2023; Revised: June 2, 2023; Accepted: June 6, 2023; Published online: June 13, 2023.

† These authors contributed equally to this work.

* Corresponding authors. Emails: tyx@nju.edu.cn (Y.T.); xuwg@nju.edu.cn (W.X.); weizh@nju.edu.cn (Z.W.)

The project was supported by the National Natural Science Foundation of China (22073046, 22173044, 62011530133), the National Key R&D Program of China (2020YFA0406104), the Fundamental Research Funds for the Central Universities (020514380256, 020514380278) and the State Key Laboratory of Analytical Chemistry for Life Science (SKLACL2217), the Natural Science Foundation of Jiangsu Province (BK20220121), Postgraduate Research & Practice Innovation Program of Jiangsu Province (KYCX22_0096).

国家自然科学基金(22073046, 22173044, 62011530133), 国家重点研发计划(2020YFA0406104), 中央高校基本科研业务费专项资金(020514380256, 020514380278), 生命科学分析化学国家重点实验室(SKLACL2217), 江苏省自然科学基金(BK20220121)及江苏省研究生科研与实践创新计划(KYCX22_0096)资助项目

Key Words: Graphene; Photothermal microscopy; Thickness-dependence; Optical absorption; Nonradiative relaxation

不同层数石墨烯的光热显微成像

都安邦†，王源璠†，魏志弘†,*，张东旭，李理，杨炜青，孙千璐，赵丽丽，徐伟高*，田玉玺*

南京大学化学化工学院，介观化学教育部重点实验室，江苏省机动车排放控制重点实验室，南京 210023

摘要：二维层状材料(石墨烯、二维过渡金属硫族化合物等)因具有独特的物理性质，引起了研究学者们的广泛关注，极大促进了化学、材料科学和凝聚态物理学的发展。开发能够探究层状材料中层数依赖的光学、电学、力学和热学特性的新技术一直是二维材料领域最活跃的研究方向之一。光热显微镜利用光激发后非辐射跃迁产生的热效应，可实现在单个颗粒或单分子水平上成像与检测，并实时捕捉微观尺度热弛豫和热传输过程。本文对比研究了石墨烯薄片在不同光热介质(空气、甘油)中随厚度变化的光热特性，发现了在两种介质中光热信号强度与样品厚度之间均存在非线性依赖关系。相比于空气介质，甘油介质中光热信号强度具有更高的对比度，且随着厚度增加表现出非单调变化。该研究提供了不同介质环境中不同层数石墨烯光吸收和热弛豫特征的细节信息，相关研究结论将为层状材料及其异质结的热学性质研究提供依据。

关键词：石墨烯；光热显微成像；层数依赖；光吸收；非辐射弛豫

中图分类号：O642

1 Introduction

The rise of graphene [1] and other monolayer materials [2–6] has opened up a new 2D world for exploring thickness-dependent physical phenomena on the atomic scale [7,8]. Taking graphite as an example, the variations in the number of layers affect the electronic structure and its optical and thermal properties [9]. To be consistent with most literature, here we use graphene flakes to represent monolayer to few-layer graphene flakes. Monolayer graphene has an amazing energy band structure with zero gap, and one of its most important properties is that its charge carriers behave as massless relativistic particles or Dirac fermions [10]. For bilayer graphene, the band gap can be modulated by applying a vertical electric field [11,12]. Meanwhile, bilayer graphene or twisted bilayer graphene exhibits abundant exotic strong correlation and topological effects, such as superconductivity, correlated insulating states, and quantum anomalous Hall effect, *etc*., which significantly contribute to the development of condensed matter physics [13–17]. In addition, multilayer graphene offers unique opportunities whose importance has grown rapidly in the past few years [18–20]. On the other hand, transition metal dichalcogenides (TMDs) from bulk material to monolayer yield an indirect-to-direct band gap evolution, which opens up abundant research interest in optoelectronics and valleytronics [21–24].

The above examples show layer-dependent electrical and optical properties of layered materials, and some exotic characteristics at the 2D limit are now being seriously considered for applications in optoelectronic devices. After photon absorption, there are multiple relaxation pathways for an excited-state electron to go back to the ground state, typical processes including fluorescence/phosphorescence emission and nonradiative pathways, such as thermal relaxation [25], carrier transport [26], graphene plasmonics [27,28], photo-acoustic generation [29], and photochemical processes [30]. Among all the above pathways, thermal relaxation is the most basic one which exists in almost all cases. Thus, understanding and control of thermal relaxation is essential in a wide range of optoelectronic applications including sensing, energy harvesting, and lighting. Recently, there are also pioneering progresses on the thermal properties of layered materials [31,32] and their heterostructures [33]. Kim's work reported that by stacking atomically thin layers of MoS_2 randomly, the heat transfer capacity of layered materials would vary greatly in different directions [31]. Zhang *et al.* achieved electrical and thermal rectification simultaneously in a $MoSe_2/WS_2$ lateral heterojunction [33]. However, a systematic study on the layer-dependent thermal relaxation properties of layered materials is still lacking. In this regard, a technique for precisely capturing and imaging the layer-number-dependent thermal properties of nanomaterials is essential for accelerating the study and exploration of graphene and related materials [34,35].

Photothermal (PT) microscopy is a new optical microscopic imaging technique that has gained extensive attention and long-term development in recent years, especially in nanomaterials and life sciences [36,37]. The principle of PT microscopy is based on the thermal lens effect [36,38], which detects the small additional divergence of the probe beam by heating-induced thermal lenses, *i.e.*, the refractive index gradient around the heated analytes (Fig. 1, right inset). Thus, PT imaging is actually an indirect detection of absorption, thermal relaxation, and transport for

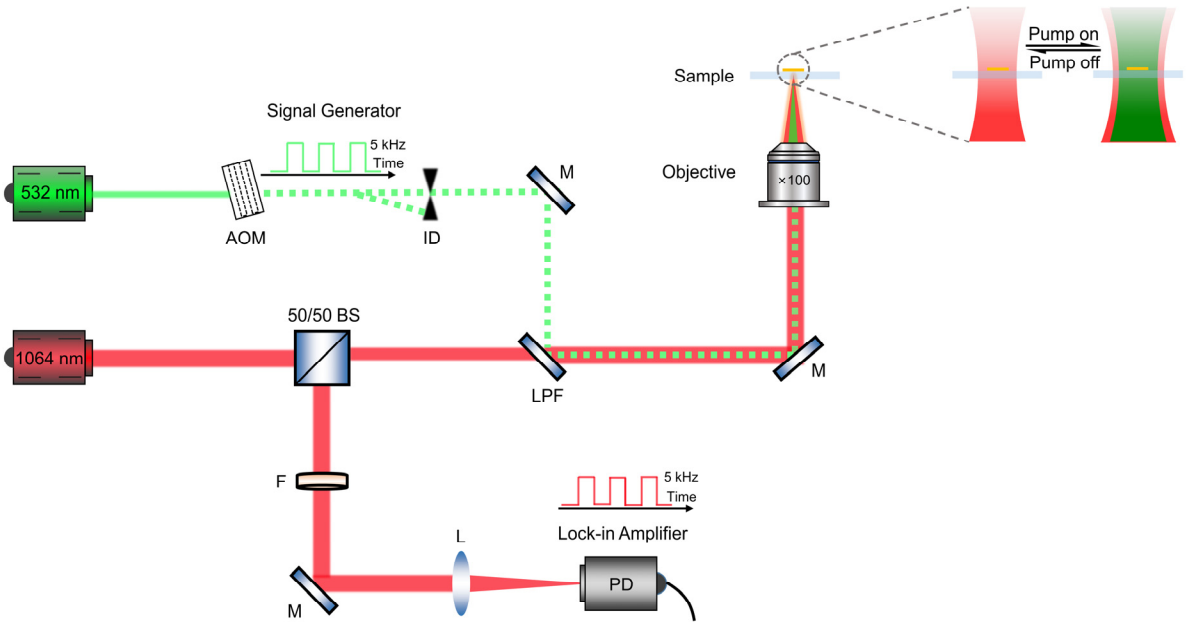

Fig. 1 Schematic diagram of the experimental setup of a home-built photothermal (PT) microscope.

AOM: acousto-optic modulators ; ID: iris diaphragm, M: mirror, BS: beam splitter, PD: photodiode, LPF: long wavelength pass filter, DM: dichroic mirror, F: filter, and L: lens.

materials with neglectable fluorescence quantum yield. In this work, we utilized PT microscopy to gain substantial insights into the thickness-dependent thermal properties of mechanically exfoliated graphene flakes. Effects on different PT media, and excitation power have been investigated and discussed. The PT intensity shows a monotonically increasing but nonlinear relationship with thickness in the air media, while in the glycerol media we found a non-monotonic PT response. This study offers insights into the thermal relaxation characteristics of graphene flakes with different thicknesses. Moreover, since optical emission and thermal relaxation are two competing processes, our work will also benefit future research related to absorption, emission, and thermal generation in layered materials and their heterostructures.

2 Experimental

2.1 Sample preparation

Kish graphite crystals were purchased from Covalent Materials Corp. We prepared mono- and multi-layer graphene flakes on glass coverslips (Fisherbrand) by a PDMS-assisted (Titan) dry transfer method after mechanical exfoliation [1,39,40]. The coverslips were cleaned with Milli-Q water (type 1), special wash solution in turn for 40 min, blown with nitrogen (≥99.999%), and exposed to plasma for 2 min not only for higher cleanliness but also for higher transferability from PDMS to the coverslip.

2.2 Micro-area Raman and transmittance spectroscopy

Raman spectra and absorption spectra were measured by a confocal micro-Raman spectrometer (HORIBA Scientific, Horiba HR Evolution, Japan). To collect the Raman spectra of mono- and multi-layer graphene flakes, a 633 nm continuous wave laser was used as the excitation source (~5 mW when arriving at the sample), and a 600 lines per millimeter grating was used to get a suitable resolution (~1 cm^{-1}). For the absorption spectra, we measured the micro-area transmittance of the sample. A 50× objective (Olympus, NA = 0.5) was applied to excite the sample, and a 100× objective (Olympus, NA = 0.9) was used to collect the signal. We used a near-infrared light (Thorlabs, SLS201L (/M), the United States) ranging from 360 nm to 2600 nm as the excitation source and a 100 lines per millimeter grating was used to obtain sufficient intensity. The transmittance spectra of a sample (T) and coverslip substrate (T_0) were collected, and then the final micro-area transmittance spectra were obtained according to T/T_0. All spectra were processed in Labspec6 software.

2.3 Optical contrast analysis

To identify the number of layers of graphene flakes, we measured the greyscale values of the samples. Color optical images (RGB format) of few-layer graphene were converted to greyscale images. Then, we measured the greyscale values of different domains in the graphene flakes. Above data processing was completed with ImageJ.

2.4 Photothermal microscopy

A schematic diagram of the optical setup and working mechanism is shown in Fig. 1, similar to the previous work [41,42]. Briefly, the PT signal arises from a slight change in the refractive index of the PT medium (air or glycerol) due to the thermal relaxation after absorption of the heating beam. The refractive index change is measured with another probe beam with a different wavelength. In this work, a 532 nm laser was used as the excitation source (heating beam), and a 1064 nm laser was used as the probe beam. The heating beam was modulated using an AOM (AA Opto Electronic, MT80-A1,5-VIS, France) at a repetition frequency of 5 kHz. The probe beam overlapped with

the heating beam on the sample through a high NA objective (UPlanFLN, NA = 0.6–1.3, Japan). Then, the backscattered light of the probe beam was collected by the same objective lens and detected by a photodiode (PD) (Femto, OE-300-IN-01-FC, Germany). The PT signal was extracted from the modulation of the scattered light by a lock-in amplifier at the same frequency as the heating beam. Optical transmission images can be collected by an optical camera (Mshot, MS23). PT images covering a whole sample area can be obtained by scanning the sample with a motorized positioning stage (TANGO 2 Desktop, Germany).

3 Results and discussion

To systematically study the layer-dependent PT properties of graphite, graphene flakes with different thicknesses were prepared using the mechanical exfoliation method [1]. Fig. 2a shows the optical image of the few-layer graphene flakes on a glass slide substrate, where the opacity increases with increasing thickness. To confirm the number of layers of graphene, we also conducted a contrast profile analysis. Two greyscale value profiles of cross-section over the sample are shown in Fig. 2b. The substrate shows a greyscale value of ~207, the first step is monolayer graphene, and the greyscale values exhibit a linear increase as the number of layers increases [43]. In addition, we characterized graphene flakes by both Raman and transmission spectroscopy (Fig. 2c,d). Fig. 2c shows typical Raman spectra of graphene with 1–4 layers acquired under the same conditions. Two main peaks at ~1580 and ~2690 cm^{-1} are the G-band and 2D-band, respectively. As we used high-quality Kish graphite crystal for mechanical exfoliation, no D-band is observed. The intensity of the G-band increases with the increase of graphene thickness. Meanwhile, the full width at half maximum of the 2D peaks gradually increases and the peak-center blue shifts as the number of graphene layers increases, which is in good agreement with the Raman spectra of few-layer graphene reported in the literature [44–46]. According to the transmission spectra (Fig. 2d), the absorbance of the monolayer graphene is ~2.0%, and the absorbance of graphene flake increases almost linearly with the number of layers exhibiting the typical features of graphite with different thicknesses [47,48]. All of the above results accurately confirm the number of layers of our samples.

Fig. 3a shows an optical microscopic image of the graphene flake on a glass slide substrate with a weak optical contrast. Fig. 3b shows a PT image of graphene in the air with a scanning area of 40 μm × 40 μm. The PT signal has a uniform distribution within sample areas with the same thickness. It should be noted that the graphene has absorption at 1064 nm which may affect the results. To exclude the effect of the probe beam, we performed the PT measurement without excitation of the heating beam and no PT signal was observed (Fig. S1, Supporting Information). A statistical analysis of the PT intensity for monolayer, bilayer and trilayer graphene is shown in Fig. 3c. The PT intensity is about 0.018 mV for monolayer, 0.028 mV for bilayer and 0.029 mV for trilayer, indicating a nonlinear relationship between PT intensity and thickness differing from the absorption of graphene [49]. This may be due to the limited

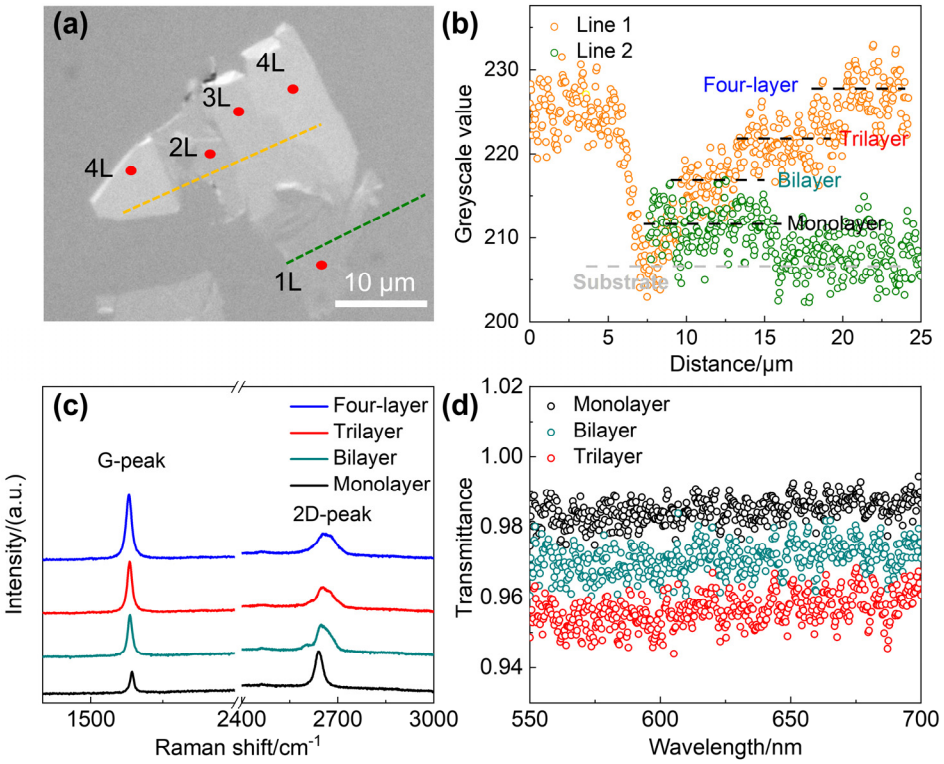

Fig. 2 (a) Optical microscopic image of a graphene flake. (b) Greyscale profile measured along the dashed line in panel a. Raman spectra (c) and transmission spectra (d) of the domains with different thicknesses.

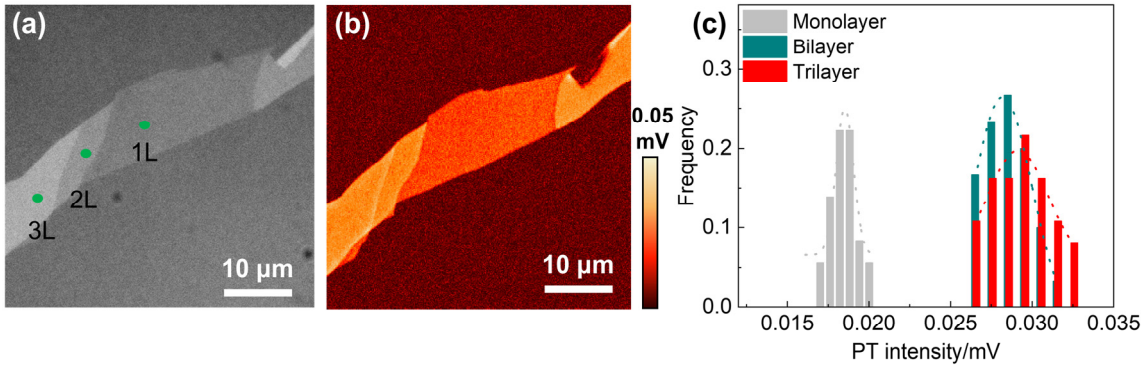

Fig. 3 Optical microscopic image (a) and PT image (b) of a graphene flake in the air. (c) Histogram of the PT intensity of monolayer, bilayer and trilayer graphene.

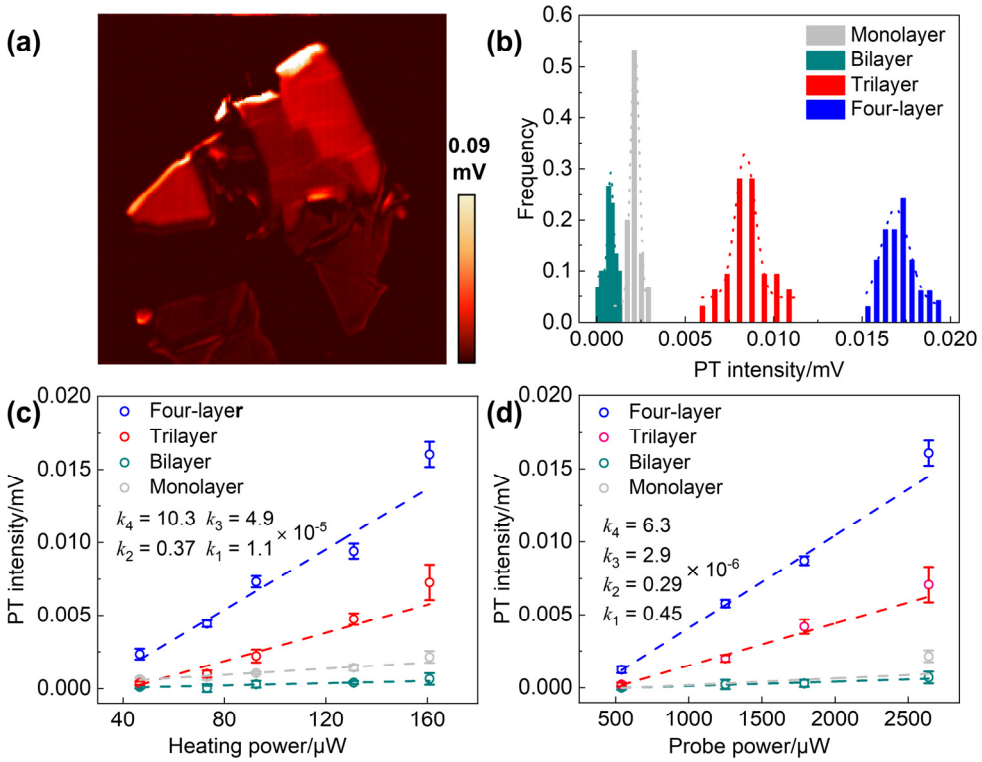

Fig. 4 (a) PT image of a graphene flake in glycerol. (b) Histogram of the PT signal of 1–4 layers graphene. The PT intensity as a function of the power of the heating (c) and probe (d) beams in glycerol.

capability of air as a PT medium to induce temporal and spatially varying refractive index changes and hence prevent the identification of small differences in the bilayer and trilayer samples [50].

In this technique, a frequency-modulated heating beam excites the absorber, which releases heat to the surrounding medium *via* nonradiative relaxation pathways [51]. The heat brings about a temperature increase in the region around the absorber, which induces a temporally and spatially modulated refractive index change. To enhance PT sensitivity, we further chose glycerol as the medium to conduct PT measurements. Fig. 4a displays a PT image of the few-layer graphene flakes in the glycerol. The statistics of the PT intensity for 1–4 layers of graphene flakes are shown in Fig. 4b. The PT intensity is about 2.2 × 10^{-3} mV for the monolayer, 7.6 × 10^{-4} mV for the bilayer, 8.5 × 10^{-3} mV for the trilayer and 1.7 × 10^{-2} mV for the four-layer. The signal to noise ratio (SNR) of graphene in different PT media was calculated to be 8.1, 13.5, 13.9 and 14.9 for 1–4 layers graphene in the air and 9.2, 3.2, 36.4 and 74.2 in the glycerol, respectively. Except for the bilayer graphene, the SNR in the glycerol is significantly higher than that in the air. Comparatively, the PT intensity in the glycerol has a nonlinear and non-monotonic relationship with thickness. If we compare these values with the PT intensity of monolayer graphene, we can see that the PT intensity of monolayer graphene is higher than that of bilayer graphene. In addition, the PT intensity of 2–4 layers shows a good linear relationship with thickness. The reason for the unusually high PT intensity of monolayer graphene could be the extremely high thermal conductivity [52,53], which eases the delivery of heat to glycerol and causes a higher

PT signal as compared to bilayer graphene. In contrast, the PT intensity of bilayer graphene is lower than expected, although it shows a good linear relationship with the trilayer and four-layer graphene. It is known that the thermal conductivity can be modulated by varying the geometric structures or folding process, and the thermal conductivity of folded graphene can be significantly decreased of its counterpart due to the phonon Umklapp and normal scattering enhancement [54,55]. Thus, we also investigated the effects of folding on the PT intensity of graphene both in the air and glycerol (Fig. S2). Similar to few-layer graphene flakes, the PT intensity of the folded plane region in the air is two times that of the monolayer graphene, while the intensity of folded plane region in the glycerol is about half that of monolayer graphene, which is consistent with the bilayer graphene.

Then, we comprehensively analyzed the relationship between the PT intensity and heating or probe power. Graphene and graphite absorb light in a wide wavelength range, but in our platform, the PT response is a differential signal between the heating light on and off, so it can be assumed that the PT signal mainly originates from the absorption of the heating beam by the sample. To avoid damaging the sample, we controlled the power of the heating and probe light within 200 and 3000 μW, respectively. The PT intensity as a function of the powers of the two laser beams is shown in Fig. 4c and d. The PT intensity showed a good linear power dependence for both laser beams. In detail, the slopes of the PT intensity of monolayer, bilayer, trilayer and four-layer to the heating power are 1.1×10^{-5}, 3.7×10^{-6}, 4.9×10^{-5}, and 10.3×10^{-5} mV·μW^{-1}, and to the probe power are 4.5×10^{-7}, 2.9×10^{-7}, 2.9×10^{-6} and 6.3×10^{-6} mV·μW^{-1}, respectively.

The PT signal comes from the heat generated by the absorption of light. Due to the extremely low fluorescence quantum yield of graphene, almost all the absorbed light is converted to heat. Thus the absorption cross-section can be calculated directly from the PT intensity because PT intensity is proportional to the absorption cross-section as discussed in the supporting information. Here we used 20 nm gold nanoparticles (Zhongkeleiming Daojin Technology Co., Ltd.) as references which also have extremely low fluorescence quantum yield. The absorption cross-section of graphene at 532 nm is calculated to be σ_{abs} (532 nm) ≈ 1.6×10^{-18} cm^2 per C atom, as described in the Supporting Information. This result is very close to the value of 5×10^{-18} cm^2 per C atom calculated based on the 2.3% absorption of graphene.

4 Conclusions

In conclusion, we have systematically investigated the thermal properties of graphene flakes with different thicknesses. We found a nonlinear relationship between PT intensity and thickness in both air and glycerol as PT media. The PT intensity of the monolayer graphene in both air and glycerol is significantly different from that of few-layer graphene flakes. A much clearer PT contrast and a non-monotonic PT response were observed in the glycerol medium. Then, we analyzed the relationship between the PT intensity and heating or probe power, demonstrating that the PT intensity exhibits a good linear relationship with the power of both laser beams. In addition, we also calculated the absorption cross-section of graphene by the PT signal. This study provides insights into the light absorption and thermal relaxation features of graphene flakes with different thicknesses, and provides a possible method to recognize the thickness by PT signals. Thanks to the various unique properties and new applications of few-layer graphene and moiré superlattices, PT microscopy will provide broader information for both future fundamental research and practical applications.

Author Contributions: Conceptualization, Y.T., W.X. and Z.W.; Sample Preparation, D.Z.; Methodology, W.Y. and Z.W.; Formal Analysis, Z.W., A.D., Y.W., Q.S., L.L. and Y.W.; Data Curation, A.D., Z.W. and Y.W.; Data Curation and Visualization, A.D., Y.W. and Z.W.; Writing – Original Draft Preparation, A.D., Y.W. and Z.W.; Writing – Review & Editing, A.D., Y.W., Z.W., Q.S. and L. Z.; Visualization and Supervision, Y.T., W.X. and Z.W.

Supporting Information: available free of charge *via* the internet at http://www.whxb.pku.edu.cn.

References

(1) Novoselov, K. S.; Geim, A. K.; Morozov, S. V.; Jiang, D. E.; Zhang, Y.; Dubonos, S. V.; Grigorieva, I. V.; Firsov, A. A. *Science* **2004,** *306*, 666. doi: 10.1126/science.1102896

(2) Splendiani, A.; Sun, L.; Zhang, Y.; Li, T.; Kim, J.; Chim, C. Y.; Galli, G.; Wang, F. *Nano Lett.* **2010,** *10*, 1271. doi: 10.1021/nl903868w

(3) Wang, X.; Du, K.; Liu, Y. Y. F.; Hu, P.; Zhang, J.; Zhang, Q.; Owen, M. H. S.; Lu, X.; Gan, C. K.; Sengupta, P.; *et al. 2D Mater.* **2016,** *3*, 031009. doi: 10.1088/2053-1583/3/3/031009

(4) Huang, B.; Clark, G.; Navarro-Moratalla, E.; Klein, D. R.; Cheng, R.; Seyler, K. L.; Zhong, D.; Schmidgall, E.; McGuire, M. A.; Cobden, D. H.; *et al. Nature* **2017,** *546*, 270. doi: 10.1038/nature22391

(5) Li, L. K.; Kim, J.; Jin, C.; Ye, G. J.; Qiu, D. Y.; da Jornada, F. H.; Shi, Z.; Chen, L.; Zhang, Z.; Yang, F.; *et al. Nat. Nanotechnol.* **2017,** *12*, 21. doi: 10.1038/nnano.2016.171

(6) Wang, L.; Xu, X.; Zhang, L.; Qiao, R.; Wu, M.; Wang, Z.; Zhang, S.; Liang, J.; Zhang, Z.; Zhang, Z.; *et al. Nature* **2019,** *570*, 91. doi: 10.1038/s41586-019-1226-z

(7) Fang, S.; Duan, S.; Wang, X.; Chen, S.; Li, L.; Li, H.; Jiang, B.; Liu, C.; Wang, N.; Zhang, L.; *et al. Nat. Photon.* **2023**, *17*, 531. doi: 10.1038/s41566-023-01181-5

(8) Chang, C.; Chen, W.; Chen, Y.; Chen, Y.; Chen, Y.; Ding, F.; Fan, C.; Fan, H.; Fan, Z.; Gong, C.; *et al. Acta Phys. -Chim. Sin.* **2021,** *37*,

2108017. [常诚, 陈伟, 陈也, 陈永华, 陈雨, 丁峰, 樊春海, 范红金, 范战西, 龚成等. 物理化学学报, **2021,** *37*, 2108017.] doi: 10.3866/PKU.WHXB202108017

(9) Geim, A. K.; Novoselov, K. S. *Nat. Mater.* **2007,** *6*, 183. doi: 10.1038/nmat1849

(10) Zhang, Y.; Tan, Y. W.; Stormer, H. L.; Kim, P. *Nature* **2005,** *438*, 201. doi: 10.1038/nature04235

(11) Zhang, Y.; Tang, T. T.; Girit, C.; Hao, Z.; Martin, M. C.; Zettl, A.; Crommie, M. F.; Shen, Y. R.; Wang, F. *Nature* **2009,** *459*, 820. doi: 10.1038/nature08105

(12) Ju, L.; Wang, L.; Cao, T.; Taniguchi, T.; Watanabe, K.; Louie, S. G.; Rana, F.; Park, J.; Hone, J.; Wang, F.; *et al. Science* **2017,** *358*, 907. doi: 10.1126/science.aam9175

(13) Cai, L.; Yu, G. *Adv. Mater.* **2021,** *33*, 2004974. doi: 10.1002/adma.202004974

(14) Cao, Y.; Rodan-Legrain, D.; Rubies-Bigorda, O.; Park, J. M.; Watanabe, K.; Taniguchi, T.; Jarillo-Herrero, P. *Nature* **2020,** *583*, 821. doi: 10.1038/s41586-020-2393-7

(15) Lin, M.; Feng, M.; Wu, J.; Ran, F.; Chen, T.; Luo, W.; Wu, H.; Han, W.; Zhang, X.; Liu, X.; *et al. Research* **2022,** *2022*, 9819373. doi: 10.34133/2022/9819373

(16) Liu, M.; Wang, L.; Yu, G. *Adv. Sci.* **2022,** *9*, 2103170. doi: 10.1002/advs.202103170

(17) Xiao, Y.; Liu, J.; Fu, L. *Matter* **2020,** *3*, 1142. doi: 10.1016/j.matt.2020.07.001

(18) Haigh, S. J.; Gholinia, A.; Jalil, R.; Romani, S.; Britnell, L.; Elias, D. C.; Novoselov, K. S.; Ponomarenko, L. A.; Geim, A. K.; Gorbachev, R. *Nat. Mater.* **2012,** *11*, 764. doi: 10.1038/Nmat3386

(19) No, Y. S.; Choi, H. K.; Kim, J. S.; Kim, H.; Yu, Y. J.; Choi, C. G.; Choi, J. S. *Sci. Rep.* **2018,** *8*, 571. doi: 10.1038/s41598-017-19084-1

(20) Ohta, T.; Bostwick, A.; McChesney, J. L.; Seyller, T.; Horn, K.; Rotenberg, E. *Phys. Rev. Lett.* **2007,** *98*, 206802. doi: 10.1103/PhysRevLett.98.206802

(21) Lu, X.; Chen, X.; Dubey, S.; Yao, Q.; Li, W.; Wang, X.; Xiong, Q.; Srivastava, A. *Nat. Nanotechnol.* **2019,** *14*, 426. doi: 10.1038/s41565-019-0394-1

(22) Seyler, K. L.; Rivera, P.; Yu, H.; Wilson, N. P.; Ray, E. L.; Mandrus, D. G.; Yan, J.; Yao, W.; Xu, X. *Nature* **2019,** *567*, 66. doi: 10.1038/s41586-019-0957-1

(23) Unuchek, D.; Ciarrocchi, A.; Avsar, A.; Sun, Z.; Watanabe, K.; Taniguchi, T.; Kis, A. *Nat. Nanotechnol.* **2019,** *14*, 1104. doi: 10.1038/s41565-019-0559-y

(24) Yu, H.; Wang, Y.; Tong, Q.; Xu, X.; Yao, W. *Phys. Rev. Lett.* **2015,** *115*, 187002. doi: 10.1103/PhysRevLett.115.187002

(25) Chen, Q.; Zhao, J.; Cheng, H.; Qu, L. *Acta Phys. -Chim. Sin.* **2021,** *37*, 2101020. [陈清, 赵健, 程虎虎, 曲良体. 物理化学学报, **2021,** *37*, 2101020.] doi: 10.3866/PKU.WHXB202101020

(26) Chen, Y.; Chen, Z. *Acta Phys. -Chim. Sin.* **2020,** *36*, 1904025. [陈尧, 陈政. 物理化学学报, **2020,** *36*, 1904025.] doi: 10.3866/PKU.WHXB201904025

(27) Bandurin, D. A.; Monch, E.; Kapralov, K.; Phinney, I. Y.; Lindner, K.; Liu, S.; Edgar, J. H.; Dmitriev, I. A.; Jarillo-Herrero, P.; Svintsov, D.; *et al. Nat. Phys.* **2022,** *18*, 462. doi: 10.1038/s41567-021-01494-8

(28) Ni, G. X.; Wang, L.; Goldflam, M. D.; Wagner, M.; Fei, Z.; McLeod, A. S.; Liu, M. K.; Keilmann, F.; Ozyilmaz, B.; Neto, A. H. C.; *et al. Nat. Photon.* **2016,** *10*, 244. doi: 10.1038/Nphoton.2016.45

(29) Tian, Y.; Tian, H.; Wu, Y. L.; Zhu, L. L.; Tao, L. Q.; Zhang, W.; Shu, Y.; Xie, D.; Yang, Y.; Wei, Z. Y.; *et al. Sci. Rep.* **2015,** *5*, 10582. doi: 10.1038/srep10582

(30) Chhowalla, M.; Shin, H. S.; Eda, G.; Li, L. J.; Loh, K. P.; Zhang, H. *Nat. Chem.* **2013,** *5*, 263. doi: 10.1038/nchem.1589

(31) Kim, S. E.; Mujid, F.; Rai, A.; Eriksson, F.; Suh, J.; Poddar, P.; Ray, A.; Park, C.; Fransson, E.; Zhong, Y.; *et al. Nature* **2021,** *597*, 660. doi: 10.1038/s41586-021-03867-8

(32) Kong, Y.; Li, X.; Wang, L.; Zhang, Z.; Feng, X.; Liu, J.; Chen, C.; Tong, L.; Zhang, J. *ACS Nano* **2022,** *16*, 11338. doi: 10.1021/acsnano.2c04984

(33) Zhang, Y.; Lv, Q.; Wang, H.; Zhao, S.; Xiong, Q.; Lv, R.; Zhang, X. *Science* **2022,** *378*, 169. doi: 10.1126/science.abq0883

(34) Wang, Y.; Kim, J. C.; Li, Y.; Ma, K. Y.; Hong, S.; Kim, M.; Shin, H. S.; Jeong, H. Y.; Chhowalla, M. *Nature* **2022,** *610*, 61. doi: 10.1038/s41586-022-05134-w

(35) Ergoktas, M. S.; Soleymani, S.; Kakenov, N.; Wang, K. Y.; Smith, T. B.; Bakan, G.; Balci, S.; Principi, A.; Novoselov, K. S.; Ozdemir, S. K.; *et al. Science* **2022,** *376*, 184. doi: 10.1126/science.abn6528

(36) Adhikari, S.; Spaeth, P.; Kar, A.; Baaske, M. D.; Khatua, S.; Orrit, M. *ACS Nano* **2020,** *14*, 16414. doi: 10.1021/acsnano.0c07638

(37) Gaiduk, A.; Yorulmaz, M.; Ruijgrok, P. V.; Orrit, M. *Science* **2010,** *330*, 353. doi: 10.1126/science.1195475

(38) Yang, W.; Wei, Z.; Nie, Y.; Tian, Y. *J. Phys. Chem. Lett.* **2022,** *13*, 9618. doi: 10.1021/acs.jpclett.2c02228

(39) Xu, W.; Liu, W.; Schmidt, J. F.; Zhao, W.; Lu, X.; Raab, T.; Diederichs, C.; Gao, W.; Seletskiy, D. V.; Xiong, Q. *Nature* **2017,** *541*, 62. doi: 10.1038/nature20601

(40) Li, H.; Li, H.; Wang, X.; Nie, Y.; Liu, C.; Dai, Y.; Ling, J.; Ding, M.; Ling, X.; Xie, D.; *et al. Nano Lett.* **2021,** *21*, 6773. doi: 10.1021/acs.nanolett.1c01356

(41) Yang, W.; Li, M.; Xie, M.; Nie, Y.; Du, A.; Tian, Y. *Rev. Sci. Instrum.* **2021,** *92*, 083701. doi: 10.1063/5.0048239

(42) Yang, W.; Li, M.; Xie, M.; Tian, Y. *J. Phys. Chem. Lett.* **2023,** *14*, 3506. doi: 10.1021/acs.jpclett.3c00491

(43) Li, H.; Wu, J. M. T.; Huang, X.; Lu, G.; Yang, J.; Lu, X.; Zhang, Q.

H.; Zhang, H. *ACS Nano* **2013,** *7*, 10344. doi: 10.1021/nn4047474

(44) Graf, D.; Molitor, F.; Ensslin, K.; Stampfer, C.; Jungen, A.; Hierold, C.; Wirtz, L. *Nano Lett.* **2007,** *7*, 238. doi: 10.1021/nl061702a

(45) Hao, Y.; Wang, Y.; Wang, L.; Ni, Z.; Wang, Z.; Wang, R.; Koo, C. K.; Shen, Z.; Thong, J. T. L. *Small* **2010,** *6*, 195. doi: 10.1002/smll.200901173

(46) Ferrari, A. C.; Meyer, J. C.; Scardaci, V.; Casiraghi, C.; Lazzeri, M.; Mauri, F.; Piscanec, S.; Jiang, D.; Novoselov, K. S.; Roth, S.; *et al.* *Phys. Rev. Lett.* **2006,** *97*, 187401. doi: 10.1103/PhysRevLett.97.187401

(47) Bonaccorso, F.; Sun, Z.; Hasan, T.; Ferrari, A. C. *Nat. Photon.* **2010,** *4*, 611. doi: 10.1038/Nphoton.2010.186

(48) Li, W.; Cheng, G.; Liang, Y.; Tian, B.; Liang, X.; Peng, L.; Walker, A. R. H.; Gundlach, D. J.; Nguyen, N. V. *Carbon* **2016,** *99*, 348. doi: 10.1016/j.carbon.2015.12.007

(49) Nair, R. R.; Blake, P.; Grigorenko, A. N.; Novoselov, K. S.; Booth, T. J.; Stauber, T.; Peres, N. M. R.; Geim, A. K. *Science* **2008,** *320*, 1308. doi: 10.1126/science.1156965

(50) Gaiduk, A.; Ruijgrok, P. V.; Yorulmaz, M.; Orrit, M. *Chem. Sci.* **2010,** *1*, 343. doi: 10.1039/c0sc00210k

(51) Ding, T.; Hou, L.; Meer, H. V. D.; Alivisatos, A. P.; Orrit, M. *J. Phys. Chem. Lett.* **2016,** *7*, 2524. doi: 10.1021/acs.jpclett.6b00964

(52) Ghosh, S.; Bao, W.; Nika, D. L.; Subrina, S.; Pokatilov, E. P.; Lau, C. N.; Balandin, A. A. *Nat. Mater.* **2010,** *9*, 555. doi: 10.1038/Nmat2753

(53) Li, H.; Ying, H.; Chen, X.; Nika, D. L.; Cocemasov, A. I.; Cai, W.; Balandin, A. A.; Chen, S. *Nanoscale* **2014,** *6*, 13402. doi: 10.1039/c4nr04455j

(54) Gao, J.; Si, C.; Yang, Y. R.; Cao, B. Y.; Wang, X. D. *ECS J. Solid State Sci. Technol.* **2020,** *9*, 093005. doi: 10.1149/2162-8777/aba7fb

(55) Ouyang, T.; Chen, Y.; Xie, Y.; Stocks, G. M.; Zhong, J. *Appl. Phys. Lett.* **2011,** *99*, 233101. doi: 10.1063/1.3665184